Cyclic 100-ka (glacial-interglacial) migration of subseafloor redox zonation on the Peruvian shelf

Sergio Contreras[a,b,1], Patrick Meister[a], Bo Liu[a], Xavier Prieto-Mollar[c], Kai-Uwe Hinrichs[c], Arzhang Khalili[a,d], Timothy G. Ferdelman[a], Marcel M. M. Kuypers[a], and Bo Barker Jørgensen[a,e]

[a]Department of Biogeochemistry, Max Planck Institute for Marine Microbiology, D-28359 Bremen, Germany; [b]Department of Geology and Planetary Science, University of Pittsburgh, Pittsburgh, PA 15260-3332; [c]Organic Geochemistry Group, MARUM-Center for Marine Environmental Sciences and Department of Geosciences, University of Bremen, D-28359 Bremen, Germany; [d]Earth and Space Sciences, Jacobs University Bremen, D-28759 Bremen, Germany; and [e]Department of Bioscience, Center for Geomicrobiology, Aarhus University, DK-8000 Aarhus C, Denmark

Edited by John M. Hayes, Woods Hole Oceanographic Institution, Woods Hole, MA, and approved August 14, 2013 (received for review April 3, 2013)

The coupling of subseafloor microbial life to oceanographic and atmospheric conditions is poorly understood. We examined diagenetic imprints and lipid biomarkers of past subseafloor microbial activity to evaluate its response to glacial-interglacial cycles in a sedimentary section drilled on the Peruvian shelf (Ocean Drilling Program Leg 201, Site 1229). Multiple and distinct layers of diagenetic barite and dolomite, i.e., minerals that typically form at the sulfate–methane transition (SMT), occur at much shallower burial depth than the present SMT around 30 meters below seafloor. These shallow layers co-occur with peaks of ^{13}C-depleted archaeol, a molecular fossil of anaerobic methane-oxidizing Archaea. Present-day, non-steady state distributions of dissolved sulfate also suggest that the SMT is highly sensitive to variations in organic carbon flux to the surface shelf sediments that may lead to shoaling of the SMT. Reaction-transport modeling substantiates our hypothesis that shallow SMTs occur in response to cyclic sediment deposition with a high organic carbon flux during interglacials and a low organic carbon flux during glacial stages. Long diffusion distances expectedly dampen the response of deeply buried microbial communities to changes in sediment deposition and other oceanographic drivers over relatively short geological time scales, e.g., glacial-interglacial periods. However, our study demonstrates how dynamically sediment biogeochemistry of the Peru Margin has responded to glacial-interglacial change and how these changes are now preserved in the geological record. Such changes in subsurface biogeochemical zonation need to be taken into account to assess the role of the subseafloor biosphere in global element and redox cycling.

deep biosphere | paleodiagenetic | methane oxidation front | biogeochemical cycles

Microbial life beneath the ocean reacts to and alters the organic matter and sediment deposited on the seafloor and buried over geological time scales of millennia or more. This subseafloor biosphere mineralizes buried organic matter, changes the geochemical gradients, and affects the precipitation or dissolution of minerals (1–3). Discrete zones of microbial abundance and activity develop (4–7) where sulfate (SO_4^{2-}) diffusing downward from the overlying seawater intersects with upward diffusing methane (CH_4). Here the anaerobic oxidation of methane (AOM) is coupled to sulfate reduction (5, 8), and both compounds become depleted in this sulfate methane transition (SMT). The SMT is typically located within the top few meters to tens of meters below seafloor in continental shelf and slope sediments. Under steady state conditions, i.e., when the rates of both organic and bulk sedimentation remain constant and the quality of the deposited organic matter is uniform over time, no significant change occurs in the fluxes of dissolved methane and sulfate, and the SMT remains at a constant depth beneath the seafloor (8, 9). Sedimentation and organic carbon flux, however, are seldom constant over time. Especially at ocean margins where the organic matter flux to the seafloor is large and variable, oceanographic changes may result in a strong response of subseafloor methane and sulfate gradients. For example, high sedimentation rates and high organic carbon fluxes lead to high microbial activity and, over time, to a shallow SMT (10). A lowered deposition rate of organic matter will reduce microbial activity and cause a downward migration of the SMT.

The SMT depth is therefore controlled by past environmental changes that affect the rate of sediment deposition and burial and, thus, affect the amount and quality of organic matter that today serves as substrate for microbial processes in the subsurface (11). Pore water analyses and microbiological studies provide information on the current metabolic processes (5–7), but the factors controlling the SMT depth over geological time are not well constrained.

Changes in the depth of the SMT as a result of variations in the flux of methane and sulfate leave diagenetic imprints, such as iron sulfides, barium sulfate (barite) or calcium carbonates (3, 9, 12, 13), and anomalous, non-steady state distributions in pore water chemistry (3, 9, 14). Carbon isotope signatures in diagenetic dolomites from a sedimentary sequence recovered from the Peru Margin suggested that biogeochemical conditions at the SMT are subject to strong variations over time (15). Regularly spaced diagenetic dolomite layers were interpreted as a consequence of periodic upward and downward migration of the SMT triggered by glacial-interglacial variation in sediment deposition (16). However, the mechanisms that drive the upward or downward shifts of the SMT and lead to episodic precipitation of diagenetic minerals remained unclear.

Significance

Microbial life beneath the seafloor affects global-scale biogeochemical processes in the ocean, including the carbon and nutrient cycles. Although considered a stable ecosystem, dynamic interaction of this deep biosphere with climate and ocean chemistry remains poorly understood. We used high-resolution geochemical tools to study the sediment archive of the Peru continental shelf and discovered signatures of past changes in subseafloor microbial oxidation of methane. A transient reaction-transport model was used to reconstruct upward and downward migrations of the methane oxidation front according to 100-ka cyclic variations in sediment deposition. The results show for the first time how microbial life beneath the seafloor interacts with changing climate and oceanographic conditions on a glacial-interglacial time scale.

Author contributions: S.C., P.M., T.G.F., M.M.M.K., and B.B.J. designed research; S.C., P.M., and B.L. performed research; B.L., X.P.-M., K.-U.H., and A.K. contributed new reagents/analytic tools; S.C., P.M., B.L., K.-U.H., A.K., T.G.F., M.M.M.K., and B.B.J. analyzed data; and S.C., P.M., K.-U.H., T.G.F., and B.B.J. wrote the paper.

The authors declare no conflict of interest.

This article is a PNAS Direct Submission.

[1]To whom correspondence should be addressed. E-mail: contrerasser@gmail.com.

This article contains supporting information online at www.pnas.org/lookup/suppl/doi:10.1073/pnas.1305981110/-/DCSupplemental.

www.pnas.org/cgi/doi/10.1073/pnas.1305981110

We present here a high-resolution record of geochemical signatures indicative of the past location of the SMT from a sedimentary sequence drilled at Ocean Drilling Program (ODP) Site 1229 at 150 m water depth on the Peruvian continental shelf (10°59′ S, 77°57′ W; Fig. S1). We scanned entire core sections at high resolution (1 cm) using an X-ray fluorescence (XRF) scanner to screen for focused element enrichments indicative of diagenetic mineral phases, such as barite and authigenic carbonates. Total organic carbon (TOC) and lipid biomarkers indicative of microbial communities at the SMT were analyzed with a depth resolution of 20 cm (5 cm in the uppermost 5 m) and compound-specific isotopic compositions of the lipids were measured at selected depths. Based on the diagenetic and molecular fossil imprints, we identify past locations of the SMT in the subseafloor and reconstruct its migration history. To test the feasibility and to understand potential geochemical controls on an upward or downward migrating SMT, the SMT depth was simulated as a function of variable sedimentation rate and organic matter influx using a transient reactive transport model. Our results reveal how dynamically the deep biosphere reacts to changes in sediment input at the seafloor and, hence, how changes in oceanographic conditions at geological timescales may influence microbial life below the seafloor.

Geological Setting

The Peruvian shelf is characterized by high rates of primary productivity due to year-round coastal upwelling resulting in high sedimentation of organic matter. The organic matter is well preserved under low oxygen conditions and serves as a substrate for microbial activity. The subseafloor biogeochemistry of Site 1229 has probably been studied in more detail than any other marine sedimentary sequence drilled to date (e.g., 5–7, 17, 18). The 200-m-thick sedimentary sequence at Site 1229 consists of organic carbon-rich (TOC up to 8 wt %), olive-green diatom ooze with variable content of silt and clay. The average sedimentation rate over the last 340 ka is 0.07 m·ka^{-1} (19); however, radiocarbon dates place the onset of significant Holocene sedimentation *ca.* 3,000 y ago at 2.3 m below seafloor (mbsf), which yields average sedimentation rates of ~0.8 m·ka^{-1} for the most recent interglacial (20). Distinct shifts during glacial-interglacial transitions in the depositional regime of the Peruvian continental shelf have been attributed to variations in sea level stand and upwelling strength (21–23). During glacial maxima, the water depth was often as low as 30 m, compared with 150 m today, with an oxic water column unlike the oxygen minimum zone that characterizes the modern water column at Site 1229. A low sea level during glacial times resulted in low net sedimentation on the continental shelf or may even have caused sediment erosion (24). In the lithological column, erosion surfaces and/or depositional unconformities occur within thin zones of low TOC at 3, 12, 17, and 20 mbsf (25). It is unknown how much sediment may have been removed at those erosional and/or depositional unconformities but the low-TOC layers coincide mostly with glacial times (Fig. 1 *A* and *F*).

Results and Discussion

Evidence for Past Oscillation of the SMT. Present pore water profiles (25) at Site 1229 (Fig. S2) locate the SMT between 23 and 33 mbsf (*SI Text*). Distinct sedimentary layers enriched in biomarkers diagnostic of AOM and diagenetic barite and dolomite, provide independent lines of evidence for past movements of the SMT (Fig. 1). In addition to the expected occurrence of archaeol in the modern-day SMT between 25 and 27 mbsf and near 30 mbsf [average of 0.45 μg·g^{-1} dry weight of sediment (dws)], peaks in archaeol content are observed above the SMT at 17.5 mbsf (0.3 μg·g^{-1} dws) and 13 mbsf (0.6 μg·g^{-1} dws), and multiple peaks between 7 and 12 mbsf (Fig. 1*B*). Maximum concentrations (16.5 μg·g^{-1} dws) occur at 10 mbsf and are in the higher range of concentrations found at modern methane seep sites (e.g., 26–29). The low isotope values of archaeol (−71‰, −73‰, and −50‰)

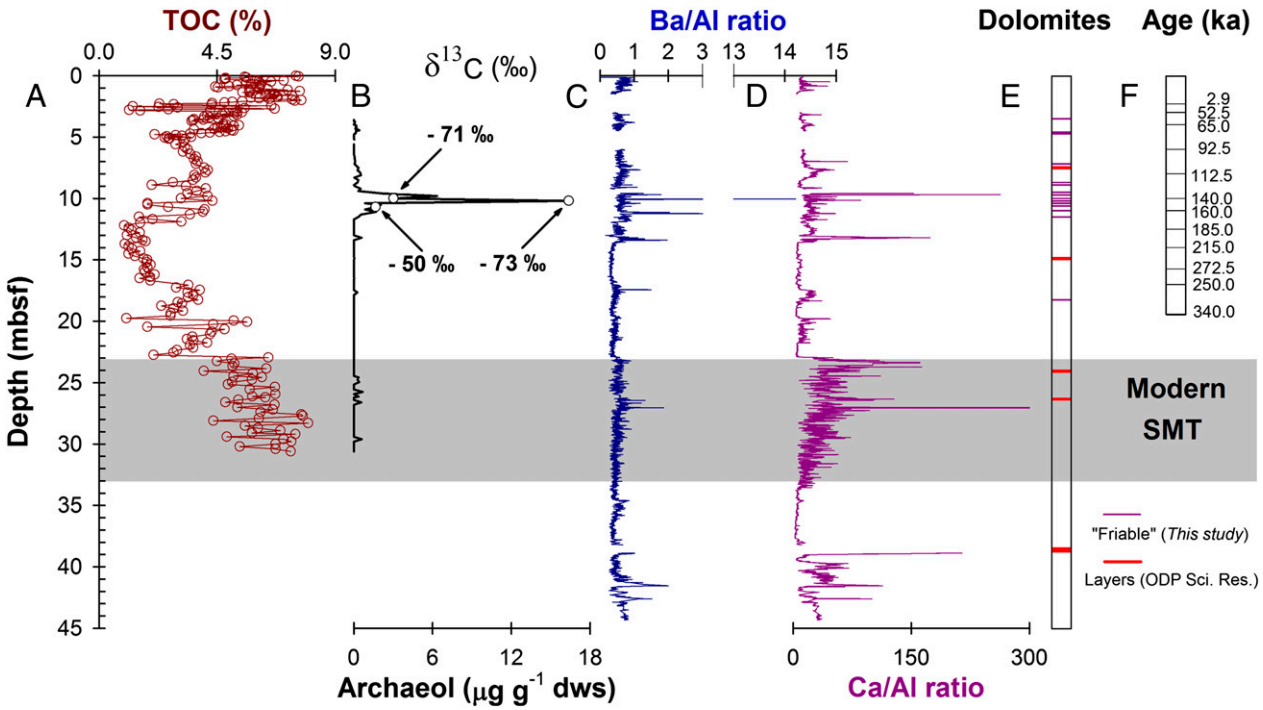

Fig. 1. Down-core records of geochemical data from ODP Site 1229. (*A*) TOC in dws. (*B*) Concentration of archaeol (micrograms per gram dws) and its $\delta^{13}C$ values (per mil VPDB). (*C*) Barium content normalized by aluminum content (Ba/Al ratio). (*D*) Calcium content normalized by aluminum content (Ca/Al ratio). (*E*) Occurrence of "friable" dolomites (this study, hole 1229E) and dolomite layers reported by Jørgensen et al. (25) for holes 1229A and 1229D. (*F*) Stratigraphic ages (ka) adopted from a chronology based on diatom assemblages and oxygen isotope values in benthic foraminifera (19). The onset of significant Holocene sedimentation at 2.9 ka is based on radiocarbon dating (20). Open bullets refer to stable carbon isotopic values in discrete samples. The gray bar shows the position of the modern SMT.

(Fig. 1*B*) suggest that this biomarker is derived from organisms using ^{13}C-depleted carbon for lipid biosynthesis, consistent with a source from methane-oxidizing Archaea (4, 26–29).

The exceptional accumulation of archaeol between 10 and 11 mbsf suggests that a SMT was stationary at relatively shallow depths for an extended time period in the past. Accordingly, an increased upward methane flux resulted in higher rates of AOM (8, 9, 11) and shoaling of the SMT. These elevated AOM rates were associated with elevated microbial biomass production as indicated by the archaeol peak at the past SMT. This core ether lipid is rather recalcitrant (30) and well preserved in sediments on geological time scales (31). In contrast, archaeol concentrations at the present SMT reflect the low modern rates of AOM observed at ODP Site 1229 (cf. 5–7), where unambiguous molecular signals of methane oxidizing communities, i.e., so-called anaerobic methane-oxidizing (ANME) Archaea, were not detected (7). Instead, the distributions of intact polar archaeal lipids, compound-specific ^{13}C ratios, and 16S-rRNA suggested that the sedimentary archaeal communities within the modern SMT are involved in the degradation of organic matter but not of methane (7). Therefore, the presence of layers exhibiting peaks of ^{13}C-depleted archaeol above the modern SMT signals the past existence of shallow microbial communities performing AOM at rates substantially greater than modern rates. Undetectable levels of archaeol in sediments between the present and the relict SMT must be due to dynamic movement of the SMT that did not remain at a specific depth long enough to cause significant accumulation of archaeol in this interval.

The distinct peak of ^{13}C-depleted archaeol at 10–11 mbsf (Fig. 1*B*) coincides with strong positive anomalies of Ba/Al and Ca/Al ratios (Fig. 1 *C* and *D*). Barium dissolved in pore water as Ba^{2+} is known to precipitate and accumulate as barite ($BaSO_4$) fronts at the SMT (2), where upward diffusing dissolved Ba^{2+} from the methane zone meets downward diffusing sulfate (Fig. S2). When situated above the present SMT, a barite front from the past will be preserved under the high sulfate concentration. Below the SMT, depletion of sulfate by microbial activity leads to an undersaturation of the pore water with respect to barite, thereby driving its dissolution and remobilization (1, 2). Distinct enrichments of Ba/Al are found below (40–45 mbsf) and above (~17 mbsf and ~13 mbsf) the present SMT, with the highest Ba peaks between 10 and 14 mbsf. Ongoing barite precipitation is inferred from the pore water profiles of sulfate and of Ba^{2+} at 26 mbsf (*SI Text* and Fig. S2) and coincides with a peak in total barium content. Dolomite layers are observed between 9 mbsf and 12 mbsf (Fig. 1*E*), i.e., at the same depth as peaks of Ca/Al and Ba/Al ratios (Fig. 1 *C* and *D*). Friable dolomites occur at similar depth as the hard-lithified beds reported from Site 1229 (25) (Fig. 1*D*). Diagenetic dolomite may form in the SMT as a result of AOM (32), which increases the pH and bicarbonate (HCO_3^-) concentration in the pore water and enhances supersaturation with respect to a variety of carbonate minerals, such as calcite, dolomite, and aragonite (15, 32, 33). Diagenetic dolomite layers or friable laminae may thus also provide signatures of past positions of the SMT.

The association of archaeol and enhanced ratios of Ba/Al and Ca/Al with the modern SMT is consistent with a causal relationship between AOM in the SMT and formation of diagenetic minerals and ^{13}C-depleted archaeal biomass. The age of the sediment at 10 mbsf is less than 140 ka based on the age model reported for this site (19). As SMT signals (i.e., the present SMTs) are by default below the depositional surface, it is reasonable to assume that the former SMT recorded at 10 mbsf was implanted at a very shallow depth during or after deposition of organic carbon-rich sediments of the last interglacial period (~125 ka ago).

Reconstructing Past SMT Migration. Collectively, peaks of archaeol, diagenetic barite, and dolomite above the modern SMT provide compelling evidence for a shallower position of the SMT in the past. Based on the regular spacing and glacial oxygen isotope values of the dolomites throughout the Pleistocene sequence at Site 1229, Meister et al. (16) suggested glacial-interglacial (100 ka) cycles as a trigger for the formation of dolomite layers at a periodically upward and downward migrating SMT. We explored this scenario by simulating sulfate and methane profiles and migration of the SMT over 100-ka cycles using a reactive transport model described by Arndt et al. (13, 34). We modeled the SMT depth assuming periodic 100-ka variations of sediment deposition. The constants and site-specific parameter values used in the model are summarized in Table 1. We applied a repeating pattern of high sedimentation rate/high-TOC interglacial sedimentation and low sedimentation rate/low-TOC glacial sedimentation. Holocene sedimentation at significant rates (0.8 m·ka^{-1} at Site 1229) began only 3 ka ago (20). Due to the delayed onset of rapid sedimentation relative to end-glacial sea level rise at this particular site, we define the start of the 100-ka cycles in our simulation 7 ka after the beginning of the interglacial time interval. An initial TOC content of 7.2 wt % was used for the periods of rapid sedimentation, which is consistent with measured TOC contents in Holocene sediments. In contrast, sedimentation rates and TOC contents during glacial times were very low; therefore an initial TOC content of 1 wt % was assumed for the interval of slow sedimentation. Rates of organic matter degradation were constrained by the organic matter reactive continuum decay function of Boudreau and Ruddick (35):

$$\mathrm{TOC}(t) = \mathrm{TOC}_0 \left[\frac{a}{(a+t)}\right]^{\nu}, \qquad [1]$$

where t is time and a and ν are fitting parameters. The parameter a describes the average lifetime of the more reactive compounds, and ν describes the distribution of poorly reactive compounds.

The model was tuned by varying the parameter ν and the length of the interval of rapid sedimentation (Table 1) to fit present-day methane and sulfate profiles (Fig. 2). The non-steady state S-shape of the sulfate profile, reached 3 ka after onset of rapid sedimentation, is very sensitive to the sedimentation rate and the length of the interval of rapid sedimentation. A time interval of 7 ka for the rapid sedimentation rate provided the best fit. Because the long-term sedimentation rate is 0.07 m·ka^{-1}, sedimentation rates during the remaining 93 ka of the cycle must have been extremely low (0.013 m·ka^{-1}).

The parameter ν strongly affected the amplitude of SMT depth variations and maximum sulfate penetration depth. A value of 0.013 was found by fitting. Such a relatively small ν in the order of 0.015 indicates a high contribution of refractory compounds to the TOC pool, and a small ν is also required to explain relatively large amounts of several wt % organic carbon that are still present >30 mbsf. The model is rather insensitive to the factor a in the organic matter pool during rapid sedimentation. For the model, we used a value of 0.1 ka, which seems realistic for freshly deposited hemipelagic sediment (cf. 35). For the slow sedimentation interval, we assumed that organic matter is poorly reactive and we used a very large value of 10^4 ka for a. This is justified because at low sea level during glacials, the sediment surface is exposed above the wave base at this shallow ODP Site as indicated by the presence of erosional surfaces and sharp TOC decreases in the sedimentary record. In addition, low organic matter content characterized glacial intervals on the Peruvian shelf (36). Rock-Eval pyrolysis (37) from samples taken at intervals with low organic carbon content (<1.5%) indicated relatively oxidized, refractory kerogen of type III that is consistent with oxic degradation of marine organic matter in shallow waters during glacials (38).

Fig. 2 shows the simulated sulfate and methane profiles during a 100-ka cycle, beginning with the onset of rapid, organic carbon-rich sedimentation. The simulation shows that multiple SMTs can form within less than 10 ka. At 7 ka after onset of rapid organic carbon-rich sedimentation, a very shallow SMT appears at 3 mbsf with an additional inverse SMT beneath. The deep "glacial" SMT slowly migrates downward to *ca.* 35 mbsf and remains for at least another thousand years until the deep sulfate is consumed. The new SMT at 3 mbsf remains stable until 20 ka after the start of

Table 1. Input constants and variables for reactive transport modeling of sulfate and methane over a 100-ka (glacial-interglacial) cycle

Parameter	Symbol	Value	Unit	Source
Monod constant (OSR)	$K_{S,\ OSR}$	0.0026	mM	(43)
Monod constant (AOM)	$K_{S,\ AOM}$	1	mM	(44)
AOM first-order rate constant	k_{AOM}	4.00E-02	y^{-1}	Fitted to SMT thickness
Temperature	t	15	°C	Based on measured temperature
Diffusion constant sulfate	D_S	0.0248	m^2/y	(39)
Diffusion constant methane	D_{CH4}	0.0388	m^2/y	(39)
Porosity	ϕ	0.7	—	Based on measured data
Density of sediment	ρ_s	2.60E+03	kg/m^3	Based on measured data
Time interval	Δt	0.2	y	Defined
Step size	Δz	0.2	m	Defined
Long-term sedimentation rate	$\acute{\omega}$	0.0675	m/ka	Age model (19)
		Interval of sedimentation		
100-ka cycles		Rapid	Slow	
Interval	dt	7	93	ka	Fitted
Sedimentation rate of interval	ω	0.786	0.013	m/ka	Based on ^{14}C data (20) and $\acute{\omega}$
Thickness	dz	5.5	1.3	m	Based on dt, ω and $\acute{\omega}$
Initial TOC	TOC_0	7.2	1	wt %	Based on measured TOC
Apparent initial age	a	0.1	10,000	ka	Defined (as discussed)
RC parameter	ν	0.015	0.015	—	Fitted
Boundary conditions		0 mbsf	200 mbsf		
Sulfate concentration	$[SO_4^{2-}]$	28	50	mM	Defined
Methane concentration	$[CH_4]$	0	zero gradient	mM	Defined (see *Materials and Methods*)

the cycle. Over the next 80 ka, the classic sulfate and methane profiles reappear and the SMT migrates back down (rapidly at first and then more slowly) to the original depth around 30 mbsf. The asymmetry in the formation of shallow SMTs and their upward and downward migration is illustrated in Fig. 3 where the depth of the SMT is plotted as a function of time over repeated 100-ka cycles. Note that a shallow SMT persists for nearly 13 ka before the glacial relaxation and deepening of the SMT begins.

Evidence of such shallow, persistent SMTs can be seen in the depositional record. High sea level stands and climatic conditions during the last interglacial led to the deposition of fresh, reactive organic matter directly over the underlying, reworked, glacial sedimentary organic matter (23), which most likely induced similar dynamic changes in the deep sediment redox zonation; therefore, the last time that a shallow SMT formed was after 125 ka ago, immediately subsequent to the end of the last interglacial.

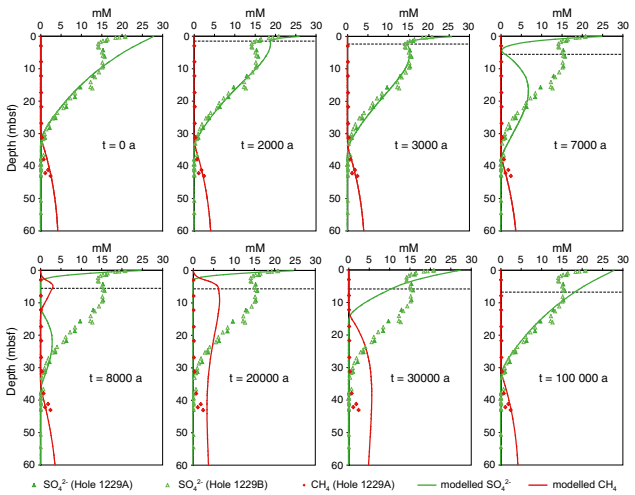

Fig. 2. Sulfate (green symbols) and methane data (red symbols) from ODP Site 1229 and simulated sulfate and methane profiles plotted vs. depth (mbsf) through a 100-ka cycle starting with the onset of a rapid sedimentation interval. Simulated distributions of sulfate (solid green line) and methane (solid red line) for (*Left* to *Right*, *Upper* to *Lower*) 0, 2, 3, 7, 8, 20, 30, and 100 ka after onset of interglacial sedimentation. The dashed horizontal line indicates the modeled accumulation of sediment through the time. The simulated sulfate and methane profiles show complex upward and downward migrations as it may have occurred on 100-ka cycles through the Pleistocene. The model reproduces present-day methane and sulfate pore water distributions 3 ka after the onset of rapid (interglacial) sedimentation; given current organic carbon fluxes to the sediment surface, the model also predicts that a non-steady state kink in the sulfate profile at 3 mbsf will become accentuated with time, and eventually form another shallow STM in ~4 ka.

Conclusions

The occurrence of focused enrichments of diagenetic barite, dolomite, and ^{13}C-depleted archaeol in sediments of ODP Site 1229 provides compelling evidence that the positions of the SMT or multiple SMTs have appeared and reappeared over the past 100 ka within the upper 35 m of Peruvian shelf sediments. Our data and model demonstrate that the SMT at Site 1229 responds dynamically with an amplitude of *ca.* 20 m to variations in sedimentation rate, organic carbon influx, and reactivity of the buried organic matter corresponding to Earth orbital 100-ka cycles. These extreme non-steady state conditions explain the unusual porewater profiles and demonstrate how dynamically microbial life beneath the seafloor can evolve at geological time scales and interact with changing climate and oceanographic conditions. The observed diagenetic enrichments constitute an archive of paleodiagenetic conditions superimposed on the sedimentary archive that documents past ocean margin changes affecting the seafloor. The occurrence and distribution of these nonlinear diagenetic signals, coupled with a quantitative understanding of how subseafloor microbial communities may respond to changing oceanographic conditions, provides predictive insight into the role of the subseafloor biosphere in global element and redox cycling.

Materials and Methods

XRF Core Scanning. We requested the archive halves of drill cores from hole E at Site 1229 (Fig. S1) in the depth interval 0–45 mbsf and deployed

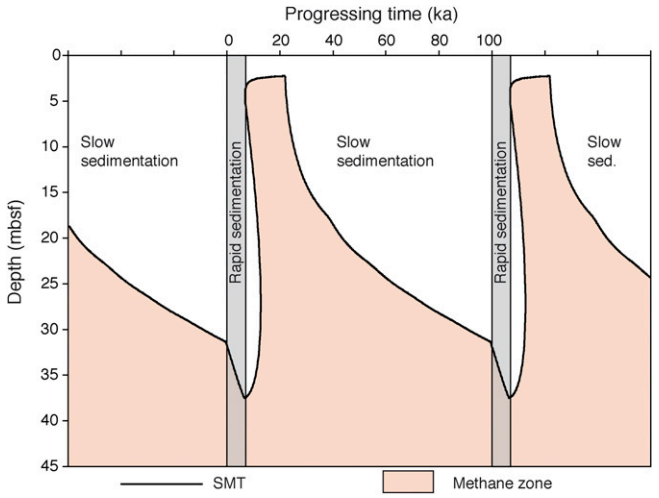

Fig. 3. Modeled distribution of the SMT during the course of 100-ka cycles starting with the onset of rapid sedimentation. Depths of SMTs that form are indicated by the dark solid line; sulfate-bearing pore waters and methane-bearing sediments are indicated by the white- and red-colored zones, respectively. The organic carbon-rich interglacial sedimentation is set for a duration of 7 ka as indicated by the gray vertical bar. Note that toward the end of the 7-ka period of rapid sedimentation, multiple SMTs appear (alternating layers of sulfate and methane as seen in Fig. 2, t = 8,000 y). The two lower SMTs converge and merge by 10–12 ka whereas the shallow SMT persists for several millennia into the period of slow sedimentation. Although the modeled cycles are offset to the glacial-interglacial cycles by 7 ka, periodic migration of the SMT is apparently associated to glacial-interglacial cycles.

nondestructive XRF core scanner analyses at the Bremen Integrated Ocean Drilling Program (IODP) Core Repository. The central sensor unit consists of a molybdenum X-ray source (3–50 kV), a Peltier-cooled PSI detector with a 125-μm beryllium window, and a multichannel analyzer with 20-eV spectral resolution. We analyzed several element intensities at 1-cm depth intervals, each measurement over an area of 1 cm^2, and looked specifically for enrichments in Ba and Ca as indicators for diagenetic barite ($BaSO_4$) and Ca/Mg carbonates.

Analysis of Discrete Sediment Samples. Discrete sediment samples were received from the IODP core repository at 5-cm depth resolution for the upper 5 m of the core and 20-cm resolution down to ~31 mbsf. TOC was calculated as the difference between total carbon measured in a Carlo Erba NA 1500 elemental analyzer and total inorganic carbon measured on a CO_2 coulometer (UIC CM 5012). Dolomites were identified from the >250-μm fraction of sieved sediments by a Philips XPERT pro X-ray diffractometer at the University of Bremen. CuKα radiation was used and the samples were scanned from 3 to 85° (2theta).

Lipid Extraction and Analysis. We performed lipid biomarker analyses to evaluate the occurrence and down-core distribution of archaeol. In brief, total lipids were extracted from freeze-dried sediment samples (1.5–2.5 g) with methanol, methanol/methylene chloride 1:1, and methylene chloride. Total lipid extracts were methylated with diazomethane and silylated with N,O-bis(trimethylsilyl)trifluoroacetamide in pyridine and analyzed by gas chromatography/mass spectrometry (GC-MS and Trace GC-MS; Thermo Finnigan). The relative abundance (micrograms per gram dws) of archaeol was estimated by peak integration in the mass chromatograms using characteristic m/z values and correcting for response factor. Repeated concentration measurements (micrograms per gram) were reproduced within ±10%.

Carbon Isotopic Composition ($\delta^{13}C$) of Archaeol. The fatty acids from the total lipid extracts of five sediment samples were separated by saponification and the neutral fraction silylated with N,O-bis(trimethylsilyl)trifluoroacetamide in pyridine. The carbon isotopic composition of trimethylsilyl ether derivative of archaeol was determined on a Trace GC Ultra gas chromatograph (Thermo Scientific) coupled to a MAT 252 Isotope Mass Spectrometer via GC Combustion Interface (Finnigan MAT) at the MARUM-Center for Marine Environmental Sciences, University of Bremen. The $\delta^{13}C$ values were corrected for additional carbon introduced during derivatization and expressed vs. Vienna PeeDee Belemnite (VPDB). The gas chromatograph was equipped with an Rxi-5MS fused-silica capillary column (30 m length, 0.25 mm inner diameter, and 0.25 μm film thickness) using helium as carrier gas at a flow of 1.2 mL/min. The temperature program used was as follows: injection at 60 °C, isothermal for 3 min, heat up to 150 °C at 10 °C/min, heat up to 320 °C at 4 °C/min, and isothermal for 25 min.

Reactive Transport Modeling. Sulfate and methane pore water profiles were simulated using a transient diffusion model approach (e.g., 10, 13) including different source/sink terms, i.e.:

$$\frac{\partial[SO_4^{2-}]}{\partial t} = -w\frac{\partial[SO_4^{2-}]}{\partial z} + \frac{D_S}{\tau^2}\frac{\partial^2[SO_4^{2-}]}{\partial z^2} - \frac{1}{2}s_{TOC} - s_{AOM} \quad [2]$$

$$\frac{\partial[CH_4]}{\partial t} = -\omega\frac{\partial[CH_4]}{\partial z} + \frac{D_{CH_4}}{\tau^2}\frac{\partial^2[CH_4]}{\partial z^2} + \frac{1}{2}s_{TOC} - s_{AOM}, \quad [3]$$

where $[SO_4^{2-}]$ and $[CH_4]$ are the concentrations of sulfate and methane (millimolars), respectively, t is time (a), ω is the sedimentation rate (m/ka), z is the depth below seafloor (meters below seafloor), and D_S and D_{CH4} are the effective diffusion constants (square meters per second) for sulfate and methane, respectively, at 15 °C. Diffusion constants are from Schulz and Zabel (39), and 15 °C is near to in situ temperature. A constant porosity (ϕ) of 0.7 was assumed, which is close to the median value of measured porosities at Site 1229. Tortuosity (τ) was calculated according to Boudreau (40) as $\tau^2 = 1–2 \ln \phi$. All parameters and units are listed in Table 1.

In situ saturation concentration of methane $[CH_4]_{sat}$ was calculated from water depth and temperature according to Yamamoto and Guinasso (41) and Wiesenburg et al. (42). The simulated methane concentrations never exceeded methane saturation at the in situ hydrostatic pressure. Different source/sink terms $s(x)$ are stoichiometrically linked to the bulk reactions of organoclastic sulfate reduction (Eq. **3**), methanogenesis (Eq. **4**), and AOM) (Eq. **5**):

$$SO_4^{2-} + 2\ CH_2O \rightarrow HS^- + 2\ HCO_3^- + H^+ \quad [4]$$

$$2\ CH_2O \rightarrow CH_4 + CO_2 \quad [5]$$

$$SO_4^{2-} + CH_4 \rightarrow HS^- + HCO_3^- + H_2O, \quad [6]$$

whereby CH_2O stands for the average composition of TOC. Rates of turnover can be calculated as decay rate S_{TOC} in mM/y, whereby S_{TOC} is calculated from the derivative of organic matter decay over time (or depth):

$$s_{TOC} = \partial\left(\frac{TOC\ \rho_S}{100\ M_C\ \phi}\right)\Big/\partial t, \quad [7]$$

where ρ_s is the density of the sediment, M is the molecular weight of carbon, and ϕ is the porosity of the sediment. To describe the decay of organic matter over time and depth, we used the reactive continuum model of Boudreau and Ruddick (35):

$$TOC(t) = TOC_0\left[\frac{a}{(a+t)}\right]^{\nu}, \quad [8]$$

where t is time and a and ν are fitting parameters. The parameter a describes the average lifetime of the more reactive compounds, and ν describes the distribution of poorly reactive compounds. As described in Arndt et al. (34), electron acceptor limitation of organoclastic sulfate reduction was considered by a Monod term $[SO_4^{2-}/(SO_4^{2-} + K_s)]$ with a K_s of 1 mM. However, we believe that this value is too high as it would result in a strong inhibition of sulfate reduction near the sediment surface. Tarpgaard et al. (43) demonstrate that a high-affinity sulfate reduction pathway exists, and their value of K_S = 0.0026 mM seems more realistic. Likewise, rates of AOM depend on a Monod-type kinetic function:

$$s_{AOM} = k_{AOM}\ [CH_4]\frac{[SO_4^{2-}]}{K_{S,AOM} + [SO_4^{2-}]}, \quad [9]$$

with a Monod constant $K_{S,AOM}$ of 1 mM (44). The k_{AOM} strongly affects the thickness of the overlap zone between methane and sulfate, and we found a value of 4×10^{-3} to fit with the overlap zone observed at Peru Margin Site 1229. According to Knab et al. (45), the thermodynamic drive was not observed to "regulate the AOM rates but only to limit the feasibility of the AOM-SRR process through a thermodynamic threshold."

According to the drilled depth at Site 1229, a domain size of 200 m was chosen for the model. Boundary conditions were 0 mM CH_4 and 28 mM SO_4^{2-}

at the sediment water interface. A fixed SO_4^{2-} concentration of 50 mM at the lower domain boundary is due to hypersaline brine, present at greater depth at site 1229. The 0 mM/m lower boundary condition for methane means that no methane is transported in or out of the domain. However, this condition is not relevant for the outcome of the model because sulfate is fixed at 50 mM and methane never reaches the lower domain boundary.

The sulfate and methane profiles determined by Eqs. **1** and **2** were simulated using a Lattice Boltzmann Method (46) following the same procedure as described in Meister et al. (10).

ACKNOWLEDGMENTS. We thank the ODP Leg 201 Shipboard Scientific Party for providing sediment samples and pore water data. Thanks also go to Michèle Watat, Thomas Max, and Gabriele Klockgether for their assistance at Max Planck Institute (MPI), Bremen. Ursula Röhl, Vera Lukies, and Walter Hale provided assistance during XRF scanning at the Bremen IODP core repository. Sediment cores and samples were graciously provided by IODP. Discussions with Susanne Henkel and Hans Røy were stimulating and constructive. The project was financed by the MPI for Marine Microbiology, Bremen, the Marie-Curie Research Training Network Greenhouse Gas Removal Apprenticeship and Student Program, the German National Science Foundation IODP Focus Program, and the Swiss National Science Foundation (SNF).

1. Torres ME, Brumsack HJ, Bohrmann G, Emeis KC (1996) Barite fronts in continental margin sediments: A new look at barium remobilization in the zone of sulfate reduction and formation of heavy barites in diagenetic fronts. *Chem Geol* 127:125–139.
2. Dickens GR (2001) Sulfate profiles and barium fronts in sediment on the Blake Ridge: Present and past methane fluxes through a large gas hydrate reservoir. *Geochim Cosmochim Acta* 65:529–543.
3. Riedinger N, et al. (2005) Diagenetic alteration of magnetic signals by anaerobic oxidation of methane related to a change in sedimentation rate. *Geochim Cosmochim Acta* 69:4117–4126.
4. Bian L, et al. (2001) Algal and archaeal polyisoprenoids in a recent marine sediment: Molecular isotopic evidence for anaerobic oxidation of methane. *Geochem Geophys Geosyst*, 10.1029/2000GC000112.
5. D'Hondt S, et al. (2004) Distributions of microbial activities in deep subseafloor sediments. *Science* 306(5705):2216–2221.
6. Parkes RJ, et al. (2005) Deep sub-seafloor prokaryotes stimulated at interfaces over geological time. *Nature* 436(7049):390–394.
7. Biddle JF, et al. (2006) Heterotrophic Archaea dominate sedimentary subsurface ecosystems off Peru. *Proc Natl Acad Sci USA* 103(10):3846–3851.
8. Borowski WS, Paull CK, Ussler W (1996) Marine pore-water sulfate profiles indicate in situ methane flux from underlying gas hydrate. *Geology* 24:655–658.
9. Hensen C, et al. (2003) Control of sulfate pore-water profiles by sedimentary events and the significance of anaerobic oxidation of methane for the burial of sulfur in marine sediments. *Geochim Cosmochim Acta* 67:2631–2647.
10. Meister P, Liu B, Ferdelman TG, Jørgensen BB, Khalili A (2013) Control of sulfate and methane distributions in marine sediments by organic matter reactivity. *Geochim Cosmochim Acta* 104:183–193.
11. Jørgensen BB, Kasten S (2006) Sulfur cycling and methane oxidation. *Marine Geochemistry*, eds Schulz HD, Zabel M (Springer, Berlin), pp 271–310.
12. März C, Hoffmann J, Bleil U, de Lange GJ, Kasten S (2008) Diagenetic changes of magnetic and geochemical signals by anaerobic methane oxidation in sediments of the Zambezi deep-sea fan (SW Indian Ocean). *Mar Geol* 255:118–130.
13. Arndt S, Hetzel A, Brumsack H-J (2009) Evolution of organic matter degradation in Cretaceous black shales inferred from authigenic barite: A reaction-transport model. *Geochim Cosmochim Acta* 73:2000–2022.
14. Wehrmann LM, Arndt S, März C, Ferdelman TG, Brunner B (2013) The evolution of early diagenetic signals in Bering Sea subseafloor sediments in response to varying organic carbon deposition over the last 4.3 Ma. *Geochim Cosmochim Acta* 109: 175–196.
15. Meister P, et al. (2007) Dolomite formation in the dynamic deep biosphere: Results from the Peru Margin. *Sedimentology* 54:1007–1032.
16. Meister P, Bernasconi SM, Vasconcelos C, McKenzie JA (2008) Sea level changes control diagenetic dolomite formation in hemipelagic sediments of the Peru Margin. *Mar Geol* 252:166–173.
17. Webster G, et al. (2006) Prokaryotic community composition and biogeochemical processes in deep subseafloor sediments from the Peru Margin. *FEMS Microbiol Ecol* 58(1):65–85.
18. Lomstein BA, Langerhuus AT, D'Hondt S, Jørgensen BB, Spivack AJ (2012) Endospore abundance, microbial growth and necromass turnover in deep sub-seafloor sediment. *Nature* 484(7392):101–104.
19. Schrader H (1992) Coastal upwelling and atmospheric CO_2 changes over the last 400,000 years: Peru. *Mar Geol* 107:239–248.
20. Skilbeck CG, Fink D (2006) Data report: Radiocarbon dating and sedimentation rates for Holocene–upper Pleistocene sediments, eastern equatorial Pacific and Peru continental margin. *Proceedings of the Ocean Drilling Program*, eds Jørgensen BB, D'Hondt SL, Miller DJ (Ocean Drilling Program, College Station, TX), Vol 201, pp 1–15.
21. De Vries TJ, Schrader H (1981) Variation of upwelling/oceanic conditions during the latest Pleistocene through Holocene off the central Peruvian coast: A diatom record. *Mar Micropaleontol* 6:157–167.
22. Reinhardt L, et al. (2002) High-resolution sediment echosounding off Peru: Late Quaternary depositional sequences and sedimentary structures of a current-dominated shelf. *Mar Geophys Res* 23:335–351.
23. Contreras S, et al. (2010) A rainy northern Atacama Desert during the last interglacial. *Geophys Res Lett* 37:L23612.
24. Mollenhauer G, Schneider RR, Müller PJ, Spieß V, Wefer G (2002) Glacial/interglacial variability in the Benguela upwelling system: Spatial distribution and budgets of organic carbon accumulation. *Global Biogeochem Cycles* 16(4):1–15.
25. D'Hondt SL, Jørgensen BB, Miller DJ, Leg 201 Shipboard Scientific Party (2003) Initial reports. *Proceedings of the Ocean Drilling Program* (Ocean Drilling Program, College Station, TX), Vol 201.
26. Hinrichs K-U, Hayes JM, Sylva SP, Brewer PG, DeLong EF (1999) Methane-consuming archaebacteria in marine sediments. *Nature* 398(6730):802–805.
27. Hinrichs K-U, Summons RE, Orphan V, Sylva SP, Hayes JM (2000) Molecular and isotopic analyses of anaerobic methane-oxidizing communities in marine sediments. *Org Geochem* 31:1685–1701.
28. Pancost RD, Sinninghe Damsté JS, de Lint S, van der Maarel MJ, Gottschal JC; The Medinaut Shipboard Scientific Party (2000) Biomarker evidence for widespread anaerobic methane oxidation in Mediterranean sediments by a consortium of methanogenic Archaea and bacteria. *Appl Environ Microbiol* 66(3):1126–1132.
29. Pancost RD, Hopmans EC, Sinninghe Damsté JS (2001) Archaeal lipids in Mediterranean cold seeps: Molecular proxies for anaerobic methane oxidation. *Geochim Cosmochim Acta* 65:1611–1627.
30. Pease TK, van Vleet ES, Barre JS, Dickins HD (1998) Simulated degradation of glyceril ethers by hydrous and flach pyrolysis. *Org Geochem* 29:979–988.
31. Bolle M-P, et al. (2000) The Paleocene-Eocene transition in the marginal northeastern Tethys (Kazakstan and Uzbekistan). *Int J Earth Sci* 89:390–414.
32. Moore TS, Murray RW, Kurtz AC, Schrag DP (2004) Anaerobic methane oxidation and the formation of dolomite. *Earth Planet Sci Lett* 229:141–154.
33. Malone MJ, Claypool G, Martin JB, Dickens GR (2002) Variable methane fluxes in shallow marine systems over geologic time: The composition and origin of pore waters and authigenic carbonates on the New Jersey shelf. *Mar Geol* 189:175–196.
34. Arndt S, Brumsack H-J, Wirtz KW (2006) Cretaceous black shales as active bioreactors: A biogeochemical model for the deep biosphere encountered during ODP Leg 207 (Demerara Rise). *Geochim Cosmochim Acta* 70:408–425.
35. Boudreau BP, Ruddick BR (1991) On a reactive continuum representation of organic matter diagenesis. *Am J Sci* 291:507–538.
36. Wefer G, Heinze SP-M, Suess E (1990) Stratigraphy and sedimentation rates from oxygen isotope composition, organic carbon content, and grain-size distribution at the Peru Upwelling Region: Holes 680B and 686B. *Proceedings of the Ocean Drilling Program*, eds Suess E, et al. (Ocean Drilling Program, College Station, TX), Vol 112, pp 355–367.
37. Tissot BP, Welte DH (1984) *Petroleum Formation and Occurrence* (Springer, New York).
38. Suess E, et al., eds (1988) *Proceedings of the Ocean Drilling Program* (Ocean Drilling Program, College Station, TX), Vol 112.
39. Schulz HD, Zabel M (2006) Quantification of early diagenesis: Dissolved constituents in marine pore water. *Marine Geochemistry*, eds Schulz HD, Zabel M (Springer, Berlin), pp 271–310.
40. Boudreau BP (1997) *Diagenetic Models and Their Implementation: Modelling Transport and Reactions in Aquatic Sediments* (Springer, Berlin).
41. Yamamoto S, Alcauskas JB, Crozler TE (1976) Solubility of methane in distilled water and seawater. *J Chem Eng Data* 21:78–80.
42. Wiesenburg DA, Guinasso NL, Jr. (1979) Equilibrium solubilities of methane, carbon monoxide, and hydrogen in water and seawater. *J Chem Eng Data* 24:356–360.
43. Tarpgaard IH, Røy H, Jørgensen BB (2011) Concurrent low- and high-affinity sulfate reduction kinetics in marine sediment. *Geochim Cosmochim Acta* 75:2997–3010.
44. Nauhaus K, Boetius A, Krüger M, Widdel F (1995) In vitro demonstration of anaerobic oxidation of methane coupled to sulfate reduction in sediment from marine gas hydrate area. *Environ Microbiol* 4:298–305.
45. Knab NJ, Dale AW, Lettmann K, Fossing H, Jørgensen BB (2008) Thermodynamic and kinetic control on anaerobic oxidation of methane in marine sediments. *Geochim Cosmochim Acta* 72:3746–3757.
46. Sukop MC, Thorne DT, Jr. (2006) *Lattice Boltzmann Modeling: An Introduction for Geoscientists and Engineers* (Springer, Heidelberg).